

UC Berkeley

UC Berkeley Previously Published Works

Title

Investigation of Potassium Storage in Layered P3-Type $K_{0.5}MnO_2$ Cathode

Permalink

<https://escholarship.org/uc/item/3h83t3bn>

Journal

Advanced Materials, 29(37)

ISSN

0935-9648

Authors

Kim, Haegyeom

Seo, Dong-Hwa

Kim, Jae Chul

et al.

Publication Date

2017-10-01

DOI

10.1002/adma.201702480

Peer reviewed

DOI: 10.1002/((please add manuscript number))

Article type: Communication

Investigation of potassium storage in layered P3-type $K_{0.5}MnO_2$ cathode

*Haegyeom Kim, Dong-Hwa Seo, Jae Chul Kim, Shou-Hang Bo, Lei Liu, Tan Shi, Gerbrand Ceder**

*Dr. H. Kim, Dr. J. Kim, Dr. S. –H. Bo, Prof. G. Ceder**

Materials Sciences Division, Lawrence Berkeley National Laboratory, Berkeley, CA 94720, USA

E-mail: gceder@berkeley.edu

*Dr. D. –H. Seo, T. Shi, Prof. G. Ceder**

Department of Materials Science and Engineering, University of California, Berkeley, CA 94720, USA

Dr. L. Liu

Department of Materials Science and Engineering, Massachusetts Institute of Technology, Cambridge, Massachusetts 02139, USA

Keywords: potassium, layered compounds, batteries, energy storage

Novel and low-cost batteries are of considerable interest for application in large-scale energy storage systems, for which the cost per cycle becomes critical. Here, we propose $K_{0.5}MnO_2$ as a potential cathode material for K-ion batteries as an alternative to Li technology. $K_{0.5}MnO_2$ has a P3-type layered structure and delivers a reversible specific capacity of ~ 100 mAh g^{-1} with good capacity retention. *In situ* X-ray diffraction analysis reveals that the material undergoes a reversible phase transition upon K extraction and insertion. In addition, first-principles calculations indicate that this phase transition is driven by the relative phase stability of different oxygen stackings with respect to the K content.

Rechargeable batteries have emerged as important devices for the storage of intermittent energy generated from renewable energy resources such as solar and wind. While Li-ion battery (LIB) technology has shown dominance in powering portable electronics and electric vehicles, it remains debatable whether the scarce resources for many of the metals in LIBs can satisfy the demands from large-scale application in grid-level storage.^[1] This uncertainty has

generated broad research interest into cost-effective alternatives. In this context, Na-ion batteries (NIBs) have been investigated as a promising option because of the abundance of Na and the similar chemistries of Na and Li systems.^[1] However, there are two critical intrinsic problems associated with NIB technology: (i) the higher standard redox potential of Na/Na⁺ usually translates into a lower working voltage than Li⁺ and (ii) graphite, a conventional anode for LIBs, cannot reversibly intercalate Na ions, instead requiring the use of hard carbon anodes.^[2] Thus, K-ion batteries (KIBs) with abundant K resources may be preferable as the standard redox potential of K/K⁺ is lower than that of Na⁺/Na, and graphite can store and release K ions.^[3]

Reversible K-ion storage in various anode materials including carbonaceous materials (*i.e.*, graphite, hard carbon, and graphene),^[3-4] metals (*i.e.*, antimony and tin),^[5] metal oxides (*i.e.*, K₂Ti₈O₁₇ and K₂Ti₄O₉),^[6] and organic materials (*i.e.*, potassium terephthalate and potassium 2,5-pyridinedicarboxylate) has been demonstrated.^[7] However, only a limited number of cathode materials for KIBs have been reported to date,^[8] making the development of appropriate cathode materials critical for practical application of KIBs. Layered transition metal oxides (TMOs) have been intensively studied for LIBs and NIBs because their close-packed structure leads to high volumetric energy density. In this respect, Vaalma *et al.* demonstrated the use of layered K_{0.3}MnO₂ as a positive electrode for K ions.^[8b] Recently, Wang *et al.* also reported the use of K_{0.7}Fe_{0.5}Mn_{0.5}O₂ nanowires as a cathode for KIBs.^[8c] These pioneering works demonstrate the potential of layered TMOs for KIBs and motivate the search for new layered TMO compounds.

In this study, we synthesized layered P3-type K_{0.5}MnO₂, and evaluated its electrochemical performance as a cathode for KIBs. Although the synthesis and structure of P3-type K_{0.5}MnO₂ have been previously reported,^[9] its K-storage properties have not yet been investigated. We further investigate the structural changes of K_{0.5}MnO₂ upon K extraction and insertion using *in situ* X-ray diffraction (XRD) coupled with electrochemical titration and

first-principles calculations. This work provides a better understanding of the underlying K-storage mechanism in layered P3-type $\text{K}_{0.5}\text{MnO}_2$ as well as insight for the design and development of novel cathode materials for KIBs.

Figure 1a presents an XRD pattern of the as-synthesized $\text{K}_{0.5}\text{MnO}_2$ and its refined profile assuming the presence of two phases with space groups of $R3m$ and $Cmcm$. The large background between 12° and 30° originates from the Kapton film used to seal the sample. The refined results indicate a P3-type layered structure ($R3m$ space group) as major phase with a small amount of orthorhombic K_xMnO_2 impurity ($\sim 6\%$) ($Cmcm$ space group). In the P3-type structure, oxygen ions form parallel layers stacked in ABBCCA sequence, with Mn ions occupying the octahedral sites, and K ions sitting in the prismatic sites between the layers of MnO_6 octahedra, as shown in Figure 1b. The hexagonal lattice parameters of the major P3- $\text{K}_{0.5}\text{MnO}_2$ phase are refined to be $a = b = 2.875 \text{ \AA}$ and $c = 19.085 \text{ \AA}$, which agrees well with the values reported in the literature.^[9] Using inductively coupled plasma-mass spectroscopy (ICP-MS) analysis, the K:Mn ratio in the sample was determined to be 0.48, close to the target composition of 0.5. The individual contributions of the target material and impurity phase to the K content in the sample cannot be distinguished using the ICP-MS technique. Therefore, we used density functional theory (DFT) calculations to determine the c lattice parameter of $\text{K}_{0.5}\text{MnO}_2$ as it is sensitive to the alkali ion concentration in layered TMOs.^[10] The calculated c lattice parameter of 19.22 \AA agrees well with the experimental result (within 1% error), which indicates that the K concentration (x) in the K_xMnO_2 sample is close to 0.5. Note that DFT calculations using the GGA+ U approach slightly overestimate lattice parameters.^[11] Examination of the powder with scanning electron microscopy (SEM) indicates that the average particle size of the as-prepared P3- $\text{K}_{0.5}\text{MnO}_2$ is 1–2 μm , as observed in Figure S1.

The K-storage properties of P3-K_{0.5}MnO₂ were investigated using cyclic voltammetry (CV) and galvanostatic measurements, with the results presented in **Figure 2**. The open-circuit voltage (OCV) of the fresh P3-K_{0.5}MnO₂ cathode is ~2.7 V (vs. K/K⁺). This OCV value is slightly lower than what is observed in K_{0.3}MnO₂ (OCV = ~3.1 V) reported by Vaalma *et al.* ^[8b], likely due to the higher K content. When scanning between 1.5 and 4.2 V (vs. K/K⁺), two strong oxidation peaks are observed at ~3.7 and 4.1 V (vs. K/K⁺), whereas the corresponding reduction peaks are less obvious (Figure 2a). In contrast, the oxidation and reduction peaks match well when scanning between 1.5 and 3.9 V, as observed in Figure 2b. These results imply that the K extraction and re-insertion processes may cause an irreversible structural change in the high-voltage region. Similar results are also obtained for galvanostatically cycling of the P3-K_{0.5}MnO₂ cathode. Figure 2c presents the voltage–capacity curves for the first four cycles at a current rate of 5 mA g⁻¹ within the voltage range of 1.5–4.2 V (vs. K/K⁺). Two distinct plateau-like features are observed at ~3.7 and ~4.1 V (vs. K/K⁺) upon charging, whereas the voltage plateaus are less pronounced in the subsequent discharge cycles. The first charge and discharge capacities are 93 and 140 mAh g⁻¹, respectively, suggesting that although ~0.39 K is removed, ~0.57 K can be reinserted. Note that higher specific capacity is achieved during discharge than during the first charge because the first charge process starts from the K-deficient phase (K_{0.5}MnO₂). When cycling between 1.5 and 3.9 V (Figure 2d), P3-K_{0.5}MnO₂ maintains a well pronounced plateau at ~3.6 V, and delivers specific capacities of ~53 and 106 mAh g⁻¹ in the first charge and discharge, respectively. These results indicate that reversible K de/intercalation can be achieved by varying the K concentration (*x*) in K_{*x*}MnO₂ between ~0.28 and ~0.72. It should be noted that the voltage profile of P3-K_{0.5}MnO₂ shares features with that of K_{0.3}MnO₂,^[8b] for which the structure is P2-type layered with an orthorhombic distortion. This implies that the potential is determined by the K content and distributions (such as K⁺/vacancy ordering) in the K⁺ layers, rather than by the polymorphism of MnO₂ stacking. In Figure 2e, we compare the capacity

retention of P3-K_{0.5}MnO₂ cycled in the two voltage ranges. The high-voltage cycling (1.5–4.2 V) leads to substantial capacity fading; the capacity of P3-K_{0.5}MnO₂ at the 20th cycle is 47 mAh g⁻¹, which is approximately 30% of its initial discharge capacity. To determine whether the poor cycling stability during the high-voltage cycling originates from a kinetic limitation or degradation of the material, we compared the cycling stability of P3-K_{0.5}MnO₂ at room temperature to that at 45 °C. As observed in Figure S2, cycling at elevated temperature does not increase the achievable capacity but leads to severe capacity fade. This finding indicates that the capacity degradation during the high-voltage cycling is likely attributable to destabilization of the charged structure of P3-K_{0.5}MnO₂. The instability of P3-K_{0.5}MnO₂ upon high-voltage cycling at 1.5–4.2 V is further confirmed from our *ex situ* XRD analysis. Figure S3 shows the XRD pattern of P3-K_{0.5}MnO₂ after 10 cycles. The typical set of diffraction peaks for the layered structure, usually observed between 15 and 30°, are missing indicating that a large portion of the phase becomes amorphized or at least loses any periodicity along the *c*-direction. In contrast, cycling between 1.5 and 3.9 V resulted in much better cycling performance for the P3-K_{0.5}MnO₂ cathode; a discharge capacity of ~81 mAh g⁻¹ (~76% of the initial discharge capacity) is maintained at the 20th cycle. At a relatively high current rate of 20 mA g⁻¹, P3-K_{0.5}MnO₂ also retains a reversible capacity of ~70 mAh g⁻¹ (~70% of the initial discharge capacity) with a coulombic efficiency of ~95% for 50 cycles when cycled at 1.5–3.9 V (Figure 2f).

The K-storage mechanism for P3-K_{0.5}MnO₂ was investigated using *in situ* XRD. **Figure 3** presents *in situ* XRD patterns (2-hour scan) collected from the P3-K_{0.5}MnO₂ cathode cycled at 2 mA g⁻¹. The (003) and (006) peaks shift to lower angles upon K extraction (Figure 3b and 3c), indicating the expansion of the MnO₂ slab distance, as is commonly observed in layered alkali-transition metal-oxide compounds.^[10, 12] More importantly, the (015) peak disappears and a new (104) peak appears to evolve at *x*~0.41 in K_{*x*}MnO₂. Unfortunately, the (104) peak overlaps with a background Al peak at ~18.5°; however, the (104) peak develops

as a noticeable shoulder-like peak upon K extraction, as observed in scan #7 in Figure 3d–f. This feature indicates a phase transition from a P3 to O3 structure as K ions removed.^[12-13] Upon further K-extraction to $x \sim 0.34$ in $K_x\text{MnO}_2$, a new set of XRD peaks to the left of the (003) and (006) peaks appears, as highlighted in Figure 3b–c, indicating the occurrence of another phase transition. We expect that these new peaks are still related to the (00 l) planes and may indicate a two-phase reaction to a phase with larger slab spacing at $0.34 > x > 0.27$. Because of the limited resolution of the *in situ* XRD and peaks from the background, we defer to explicitly determine the structure of this new phase at high state of charge and denote the phase as “X”. However, it should be emphasized that the X phase may maintain O3-like stacking as the shoulder-like (104) peak is still evident; the overall peak intensity near 18.5° at $0.34 > x > 0.27$ in $K_x\text{MnO}_2$ (e.g., #14 in Figure 3d–f) is larger than that in P3- $K_{0.5}\text{MnO}_2$ (#1), indicating superposition of the (104) peak on the Al background. The phase evolution is reversed during the discharge process with no additional phase transitions when discharging to 1.5 V, suggesting reversible K intercalation and deintercalation behavior in P3- $K_{0.5}\text{MnO}_2$. The P3-O3-X transitions can be more clearly seen in the 2D plot of the *in situ* XRD patterns presented in Figure S4.

To further validate the phase transition with respect to the K content, we computed the formation energies of P3-, O3-, and O1-type $K_x\text{MnO}_2$ structures as a function of the K content ($x = 0.25, 0.33, 0.5, 0.66$) using Density Functional Theory (DFT). The results are plotted in **Figure 4a**. We considered the P3 (ABBCCA oxygen stacking), O3 (ABCABC oxygen stacking), and O1 (ABBA oxygen stacking) structures as they can transform into each other *via* sliding of the MnO_2 slab without breaking Mn–O bonds. In Na_xMO_2 , a similar P3–O3 phase transition is experimentally observed during electrochemical cycling, and transformation to an O1 structure is sometimes observed at low Na concentrations.^[12-14] The computational results indicate that the P3-type framework has the lowest energy at high K content ($x = 0.5$ and 0.66), whereas the O3-type framework becomes stable at low K content

($x = 0.25$ and 0.33), which is consistent with observation of a P3 to O3 transition observed in the *in situ* XRD. An approximate voltage profile was also calculated from the ground state DFT energies as

$$V = -\frac{E(\text{K}_{x_1}\text{MnO}_2) - E(\text{K}_{x_2}\text{MnO}_2) - (x_2 - x_1)E(\text{K})}{(x_2 - x_1)F}, \quad [15]$$

where $E(\text{K}_x\text{MnO}_2)$ is the DFT energies of the most stable K_xMnO_2 configurations at each composition and $E(\text{K})$ is the energy of bcc K metal (space group: Im-3m). F is the Faraday constant. Figure 4 b shows calculated voltage profile of K_xMnO_2 (red line) as a function of K contents overlaid with the experimental charged/discharged voltage profile (black line). The calculated voltage profile is in a good agreement with the experimental voltage profile. The large K slab spacing ($> 4 \text{ \AA}$) between the oxide layers necessitates use of the van der Waals (vdW) correction^[16] to calculate the voltage profile. Without vdW correction the voltage is under-predicted by about 0.55 V (Figure S6).

Large alkali ions, such as Na^+ and K^+ have certain advantages over Li^+ ions. In many Li layered oxide compounds, TM ions migrate into the Li layer upon delithiation, which often results in an irreversible structural change and thus capacity degradation.^[17] Layered LiMnO_2 , for example, is almost completely converted into a spinel structure due to rapid redistribution of Mn into the Li sites.^[18] This TM migration through the intermediate tetrahedral site is assisted by Li migration into tetrahedral sites, forming $\text{TM}_{\text{tet}}\text{-Li}_{\text{tet}}$ dumbbells.^[18a, 19] Although TM migration has also been reported in Na systems, usually when more than 0.5 Na is extracted, as observed in NaFeO_2 , NaTiO_2 , and NaCrO_2 ,^[13, 20] this process is energetically more difficult than in the Li systems because the larger size of Na^+ makes it energetically less favorable to form a Na-TM dumbbell.^[19] It is highly likely that TM migration is even more difficult in K-layered oxides because of the large K ion radius. In addition, the larger K slab spacing creates highly distorted sites in the alkali layer, making TM migration less favorable, as compared to Na and Li layered materials. This explains at least in part why the structural

change upon electrochemical cycling is reversible in K_xMnO_2 for $0.27 < x < 0.70$, as demonstrated by our electrochemical results.

The data in Figure 2 indicates that the voltage range substantially affects the cyclability of the P3- $K_{0.5}MnO_2$ cathode. When charging to 4.2 V, the plateau-like voltage profile observed at ~4.1 V suggests that the material undergoes a structure change that is different from the P3-O3-X transformation. However, unlike the plateau for the O3-X transformation, this high voltage plateau is less obvious in discharge, and this irreversibility of structural evolution likely impacts the capacity retention. To better understand the nature of phase transformation occurring at ~4.1 V, we performed *in situ* XRD for two successive cycles between 1.5-4.2 V at a current rate of 7 mA g⁻¹ (Figure S5). Interestingly, the (00 l) peaks at 6.5° and 12.5° broaden while their intensity significantly decreases at the top of charge ($x < 0.27$ in K_xMnO_2). This change in the peak profile can originate from stacking faults along the c -axis. The subsequent discharge partially recovers the peak profile, but not perfectly, implying that only some of the stacking changes are reversible. This trend in the (00 l) peaks is also observed during the 2nd cycle. As a result, we expect the repeated formation and partial healing of the stacking faults or defects to result in an irreversible structure change. Thus the voltage range should be carefully tuned to extend the effective lifetime of the P3- $K_{0.5}MnO_2$ cathode.

In summary, we demonstrated P3-structured $K_{0.5}MnO_2$ as a new cathode material for KIBs. This cathode delivers a reversible capacity of ~100 mAh g⁻¹. Between 1.5 and 3.9 V, K_xMnO_2 cycles through reversible P3-O3-X phase transitions, whereas overcharging to 4.2 V leads to significant capacity loss. This combined experimental and theoretical study on layered $K_{0.5}MnO_2$ provides insight for the design of novel cathode materials and opens up a new path toward the development of high-performance KIBs.

Supporting Information

Supporting Information is available from the Wiley Online Library or from the author.

Acknowledgements

This work was supported by the Laboratory Directed Research and Development Program of Lawrence Berkeley National Laboratory under U.S. Department of Energy (Contract No. DE-AC02-05CH11231). The SEM experiment was performed at the Molecular Foundry, LBNL, supported by the Office of Science, Office of Basic Energy Sciences of the US Department of Energy (Contract No. DE-AC02-05CH11231). This work used the Extreme Science and Engineering Discovery Environment (XSEDE), which is supported by National Science Foundation grant no. ACI-1053575, and resources of the National Energy Research Scientific Computing Center (NERSC), a DOE Office of Science User Facility supported by the Office of Science of the US Department of Energy under contract no. DE-AC02-05CH11231. This research was also supported by Basic Science Research Program through the National Research Foundation of Korea (NRF) funded by the Ministry of Education (2017R1A6A3A03001850).

Received: ((will be filled in by the editorial staff))

Revised: ((will be filled in by the editorial staff))

Published online: ((will be filled in by the editorial staff))

References

- [1] a) H. Kim, H. Kim, Z. Ding, M. H. Lee, K. Lim, G. Yoon, K. Kang, *Adv. Energy Mater.* 2016, 6, 1600943; b) S.-W. Kim, D.-H. Seo, X. Ma, G. Ceder, K. Kang, *Adv. Energy Mater.* 2012, 2, 710-721; c) M. D. Slater, D. Kim, E. Lee, C. S. Johnson, *Adv. Funct. Mater.* 2013, 23, 947-958.
- [2] G. Yoon, H. Kim, I. Park, K. Kang, *Adv. Energy Mater.* 2017, 7, 1601519.
- [3] a) S. Komaba, T. Hasegawa, M. Dahbi, K. Kubota, *Electrochem. Commun.* 2015, 60, 172-175; b) Z. Jian, W. Luo, X. Ji, *J. Am. Chem. Soc.* 2015, 137, 11566-11569.
- [4] a) Z. Jian, Z. Xing, C. Bommier, Z. Li, X. Ji, *Adv. Energy Mater.* 2016, 6, 1501874; b) K. Share, A. P. Cohn, R. Carter, B. Rogers, C. L. Pint, *ACS Nano* 2016, 10, 9738-9744; c) H. Kim, G. Yoon, K. Lim, K. Kang, *Chem. Commun.* 2016, 52, 12618-12621.
- [5] a) W. D. McCulloch, X. Ren, M. Yu, Z. Huang, Y. Wu, *ACS Appl. Mater. Sci.* 2015, 7, 26158-26166; b) I. Sultana, T. Ramireddy, M. M. Rahman, Y. Chen, A. M. Glushenkov, *Chem. Commun.* 2016, 52, 9279-9282.
- [6] a) J. Han, M. Xu, Y. Niu, G.-N. Li, M. Wang, Y. Zhang, M. Jia, C. m. Li, *Chem. Commun.* 2016, 52, 11274-11276; b) B. Kishore, V. G. N. Munichandraiah, *J. Electrochem. Soc.* 2016, 163, A2551-A2554.
- [7] a) K. Lei, F. Li, C. Mu, J. Wang, Q. Zhao, C. Chen, J. Chen, *Energy Environ. Sci.* 2017; b) Q. Deng, J. Pei, C. Fan, J. Ma, B. Cao, C. Li, Y. Jin, L. Wang, J. Li, *Nano Energy* 2017, 33, 350-355.
- [8] a) A. Eftekhari, *J. Power Sources* 2004, 126, 221-228; b) C. Vaalma, G. A. Giffin, D. Buchholz, S. Passerini, *J. Electrochem. Soc.* 2016, 163, A1295-A1299; c) X. Wang, X. Xu, C. Niu, J. Meng, M. Huang, X. Liu, Z. Liu, L. Mai, *Nano Lett.* 2017, 17, 544-550; d) L. Xue, Y. Li, H. Gao, W. Zhou, X. Lü, W. Kaveevivitchai, A. Manthiram, J. B. Goodenough, *J. Am. Chem. Soc.* 2017; e) C. Zhang, Y. Xu, M. Zhou, L. Liang, H. Dong, M. Wu, Y. Yang, Y. Lei, *Adv. Funct. Mater.* 2017, 27, 1604307.
- [9] C. Delmas, C. Fouassier, *Z Anorg Allg Chem.* 1976, 420, 184-192.
- [10] R. Berthelot, D. Carlier, C. Delmas, *Nat. Mater.* 2011, 10, 74-80.

- [11] a) Y. Hinuma, Y. S. Meng, G. Ceder, *Phys. Rev. B* 2008, 77, 224111; b) V. L. Chevrier, S. P. Ong, R. Armiento, M. K. Y. Chan, G. Ceder, *Phys. Rev. B* 2010, 82, 075122.
- [12] S. Komaba, N. Yabuuchi, T. Nakayama, A. Ogata, T. Ishikawa, I. Nakai, *Inorg. Chem.* 2012, 51, 6211-6220.
- [13] S.-H. Bo, X. Li, A. J. Toumar, G. Ceder, *Chem. Mater.* 2016, 28, 1419-1429.
- [14] D. Yuan, X. Liang, L. Wu, Y. Cao, X. Ai, J. Feng, H. Yang, *Adv. Mater.* 2014, 26, 6301-6306.
- [15] M. K. Aydinol, A. F. Kohan, G. Ceder, K. Cho, J. Joannopoulos, *Phys. Rev. B* 1997, 56, 1354-1365.
- [16] S. Grimme, J. Antony, S. Ehrlich, H. Krieg, *J. Chem. Phys.* 2010, 132, 154104.
- [17] a) L. A. de Picciotto, M. M. Thackeray, W. I. F. David, P. G. Bruce, J. B. Goodenough, *Mater. Res. Bul.* 1984, 19, 1497-1506; b) Y. Shao - Horn, S. A. Hackney, A. R. Armstrong, P. G. Bruce, R. Gitzendanner, C. S. Johnson, M. M. Thackeray, *J. Electrochem. Soc.* 1999, 146, 2404-2412; c) Z. Lu, J. R. Dahn, *J. Electrochem. Soc.* 2003, 150, A1044-A1051.
- [18] a) J. Reed, G. Ceder, A. Van Der Ven *Electrochem. Solid State Lett.* 2001, 4, A78-A81; b) G. Vitins, K. West, *J. Electrochem. Soc.* 1997, 144, 2587-2592; c) R. J. Gummow, M. M. Thackeray, *J. Electrochem. Soc.* 1994, 141, 1178-1182; d) J. N. Reimers, E. W. Fuller, E. Rossen, J. R. Dahn, *J. Electrochem. Soc.* 1993, 140, 3396-3401.
- [19] S. Kim, X. Ma, S. P. Ong, G. Ceder, *Phys. Chem. Chem. Phys.* 2012, 14, 15571-15578.
- [20] a) N. Yabuuchi, H. Yoshida, S. Komaba, *Electrochemistry* 2012, 80, 716-719; b) A. Maazaz, C. Delmas, P. Hagenmuller, *J. Incl. Phenom.* 1983, 1, 45-51.

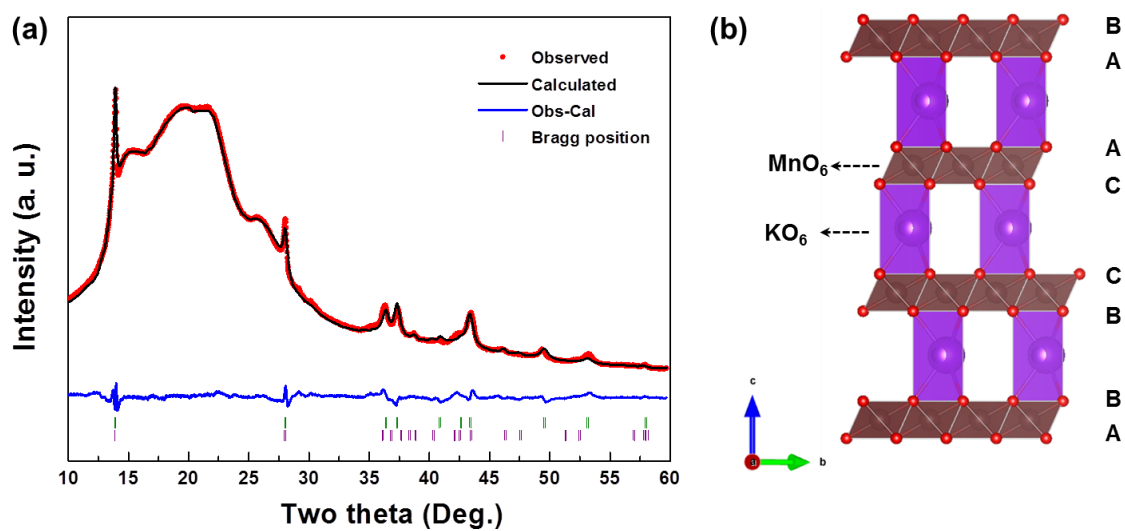


Figure 1. Structural characterization of P3- $K_{0.5}MnO_2$. (a) Rietveld-refined XRD profile of as-prepared $K_{0.5}MnO_2$. The structure was refined assuming the coexistence of a majority $R3m$ phase (green) and a minority $Cmcm$ phase (purple). $R_{wp} = 3.2$. (b) Illustration of the P3-type $K_{0.5}MnO_2$ structure.

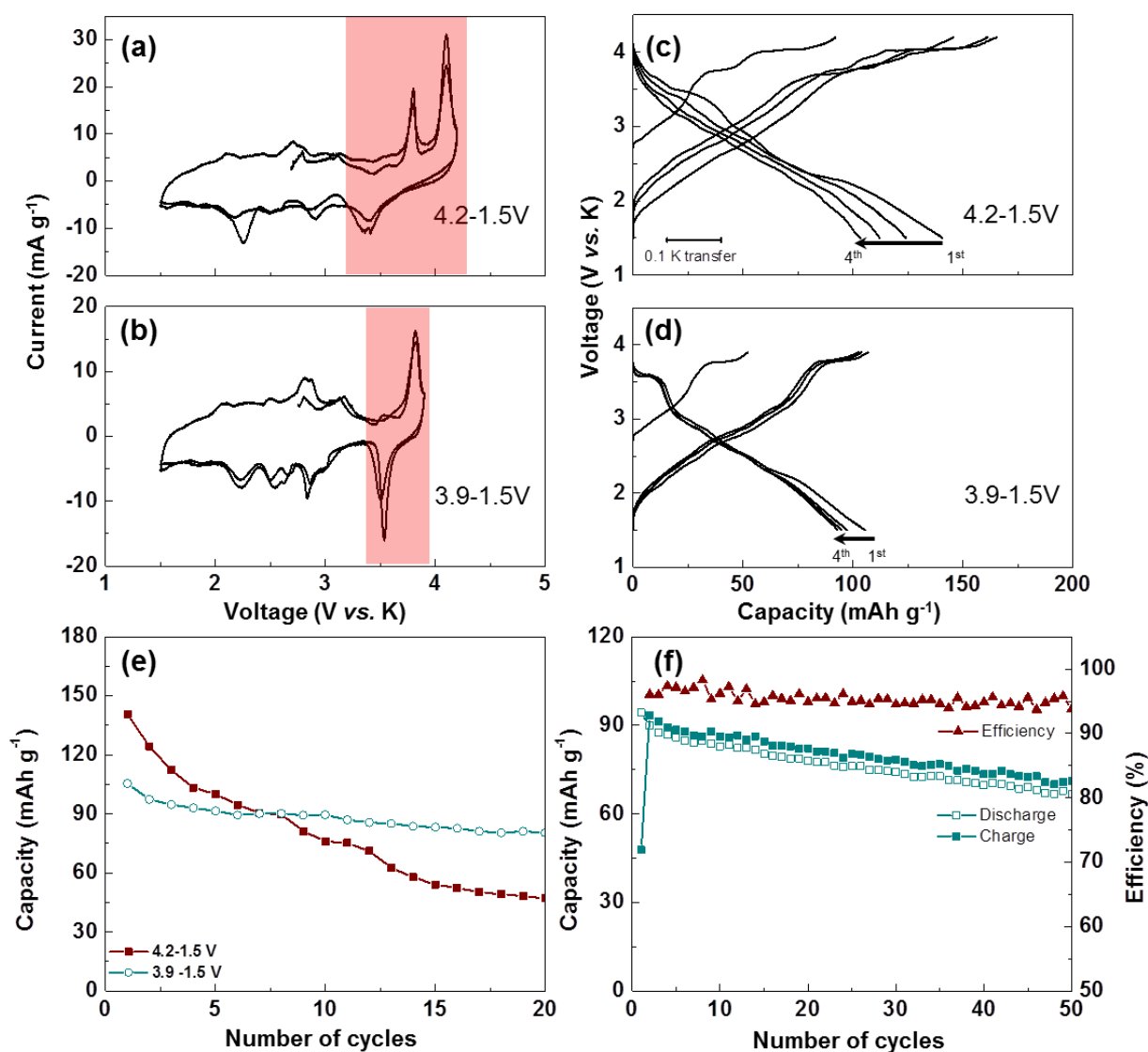


Figure 2. K-storage properties of P3- $K_{0.5}MnO_2$. (a–b) Cyclic voltammograms and (c–d) galvanostatic voltage–capacity profiles of P3-type $K_{0.5}MnO_2$ with two different voltage cutoffs. (e) Discharge capacity of P3-type $K_{0.5}MnO_2$ over 20 cycles with the two different voltage cutoffs at a current rate of $5\ mA\ g^{-1}$. (f) Cycle stability and coulombic efficiency (of the 1st discharge) of P3-type $K_{0.5}MnO_2$ at a current rate of $20\ mA\ g^{-1}$ in the range of 3.9–1.5 V (vs. K/K^+).

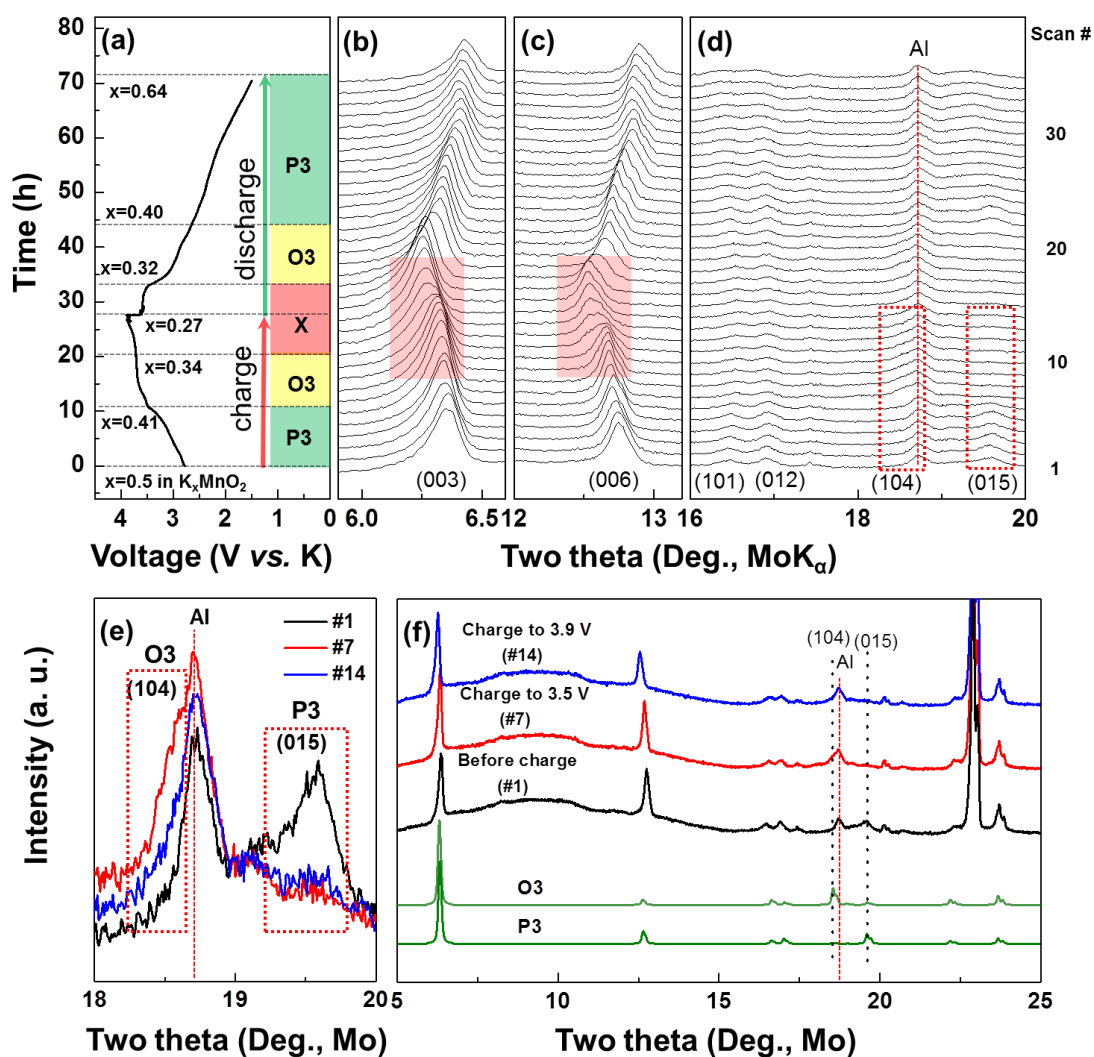


Figure 3. Structural changes of P3-K_{0.5}MnO₂ during charge and discharge. (a) Typical charge/discharge profiles of P3-type K_{0.5}MnO₂ at a current rate of 2 mA g⁻¹. (b–d) *In situ* XRD pattern taken for 2 h scanning rate per pattern. (e) XRD peak comparison of as-prepared (scan #1), scan #7, and scan #14 P3-K_{0.5}MnO₂ at 18° to 20°, in which the (104) and (015) peaks indicate O3 and P3 structures, respectively; and (f) comparison with simulated XRD patterns of the O3 and P3 structures. K ions occupy octahedral and prismatic sites in the O3 and P3 structures, respectively. The O3 structure has an ABCABC oxygen stacking sequence, whereas the P3 structure has an ABBCA oxygen stacking sequence.

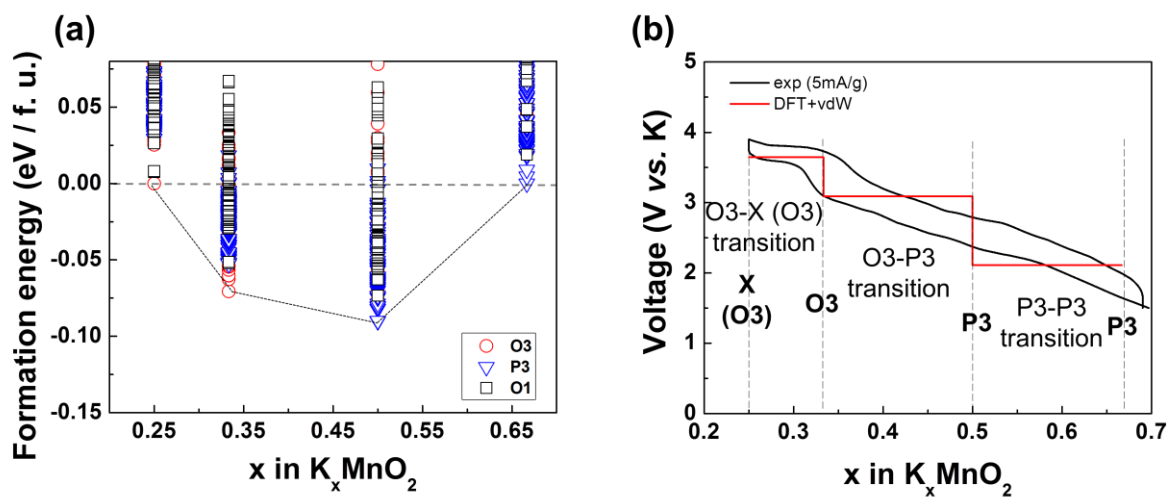


Figure 4. **a.** Formation energies of P3, O3, and O1 structures for K_xMnO_2 as a function of K content (x) obtained using *ab initio* DFT calculations. **b.** Calculated voltage plot (DFT+vdW) compared with experimentally obtained charge/discharge profiles.

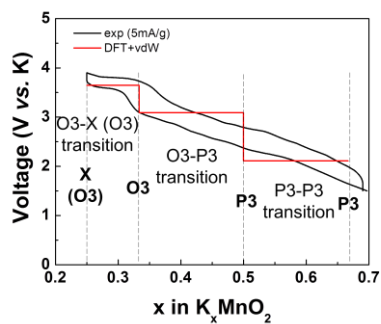
This work demonstrates K-intercalation in P3-structured $K_{0.5}MnO_2$ for the first time. It investigates the K-intercalation chemistry upon K extraction and insertion using *in situ* X-ray diffraction combined with electrochemical titration and first-principles calculations. Finally, it observes phase transitions driven by the relative phase stability of difference stacking with respect to the K content.

Keyword

potassium, layered compounds, batteries, energy storage

Dr. Haegyeom Kim, Dr. Dong-Hwa Seo, Dr. Jae Chul Kim, Dr. Shou-Hang Bo, Dr. Lei Liu, Tan Shi, Prof. Gerbrand Ceder*

Investigation of potassium storage in layered P3-type $K_{0.5}MnO_2$ cathode



Copyright WILEY-VCH Verlag GmbH & Co. KGaA, 69469 Weinheim, Germany, 2016.

Supporting Information

Investigation of potassium storage in layered P3-type $K_{0.5}MnO_2$ cathode

*Haegyeom Kim, Dong-Hwa Seo, Jae Chul Kim, Shou-Hang Bo, Lei Liu, Tan Shi, Gerbrand Ceder**

*Dr. H. Kim, Dr. J. Kim, Dr. S. –H. Bo, Prof. G. Ceder**

Materials Sciences Division, Lawrence Berkeley National Laboratory, Berkeley, CA 94720, USA

E-mail: gceder@berkeley.edu

*Dr. D. –H. Seo, T. Shi, Prof. G. Ceder**

Department of Materials Science and Engineering, University of California, Berkeley, CA 94720, USA

Dr. L. Liu

Department of Materials Science and Engineering, Massachusetts Institute of Technology, Cambridge, Massachusetts 02139, USA

Experimental section

Synthesis of P3-type $K_{0.5}MnO_2$

P3-type $K_{0.5}MnO_2$ was prepared using a conventional solid-state method. Stoichiometric amounts of K_2CO_3 (anhydrous, VWR) and Mn_2O_3 (99.9%, Sigma–Aldrich) were mixed and homogenized using a planetary ball-mill (Retsch PM200) at 300 rpm for 4 h. The resulting mixture was pelletized using uniaxial pressing and annealed at 800 °C for 12 h to crystallize the phase. After cooling, the sample was kept at 200 °C and transferred into an Ar-filled glovebox to prevent contamination from moisture.

Calculation details

All first-principles calculations were performed using the Vienna *ab initio* simulation package program^[1] with the spin-polarized GGA.^[2] We used the Perdew–Burke–Ernzerhof exchange-correlation parameterization to density functional theory^[3] and the projector-augmented wave

method.^[4] The GGA+ U approach^[5, 6] with a U value of 3.9 eV for Mn^[7] was used to correct the incomplete cancellation of the self-interaction in GGA. We used a kinetic cutoff energy of 520 eV and various k -point meshes with a grid density of 1000 per number of atoms in a supercell. All the possible K-vacancy orderings within O3-, P3-, and O1-K_xMnO₂ supercells up to nine formula units of K_xMnO₂ were created using an enumeration technique,^[8] and for each composition the 300 arrangements with the lowest electrostatic energies were calculated using GGA+ U . To describe the van der Waals interaction between oxide layers in K_xMnO₂ for the voltage prediction, the DFT-D3 scheme suggested by Grimme *et al.* was adopted.^[9]

Characterization

The structure of each sample was analyzed using XRD (Rigaku Miniflex 600) with Cu K α radiation, and the structural parameters were determined by the Rietveld method using a Highscore Plus software. The morphologies of the samples were verified using field-emission SEM (FE-SEM; Zeiss Gemini Ultra-55). The *in situ* XRD analysis was performed using a diffractometer equipped with a Mo source (Bruker D8) and a homemade *in situ* electrochemical cell with a Be window. The *in situ* cell was cycled galvanostatically using a potentiostat/galvanostat (Solartron 1287).

Electrochemical test

Electrodes were prepared by mixing as-synthesized K_{0.5}MnO₂ (80 wt%), Super P carbon black (Timcal, 10 wt%), and dry polytetrafluoroethylene (DuPont, 10 wt%) in an Ar-filled glovebox. Test cells were assembled into 2032 coin-cells in the glovebox with a two-electrode configuration using K metal counter electrodes. A separator of grade GF/F (Whatman, USA) and an electrolyte of 0.7 M KPF₆ in ethylene carbonate/diethyl carbonate (anhydrous, 1:1

volume ratio) were used. The electrochemical tests were performed on a battery testing station (Arbin Instruments) using cathode films with a loading density of $\sim 5.8 \text{ mg cm}^{-2}$.

References

- [1] G. Kresse and J. Furthmüller, *Comput. Mater. Sci.*, 1996, **6**, 15-50.
- [2] A. D. Becke, *Phys. Rev. A*, 1988, **38**, 3098-3100.
- [3] J. P. Perdew, K. Burke and M. Ernzerhof, *Phys. Rev. Lett.*, 1996, **77**, 3865-3868.
- [4] P. E. Blöchl, *Phys. Rev. B*, 1994, **50**, 17953-17979.
- [5] V. I. Anisimov, J. Zaanen and O. K. Andersen, *Phys. Rev. B*, 1991, **44**, 943-954.
- [6] S. L. Dudarev, G. A. Botton, S. Y. Savrasov, C. J. Humphreys and A. P. Sutton, *Phys. Rev. B*, 1998, **57**, 1505-1509.
- [7] A. Jain, G. Hautier, S. P. Ong, C. J. Moore, C. C. Fischer, K. A. Persson and G. Ceder, *Phys. Rev. B*, 2011, **84**, 045115.
- [8] G. L. W. Hart and R. W. Forcade, *Phys. Rev. B*, 2008, **77**, 224115.
- [9] S. Grimme, J. Antony, S. Ehrlich and H. Krieg, *J. Chem. Phys.*, 2010, **132**, 154104.

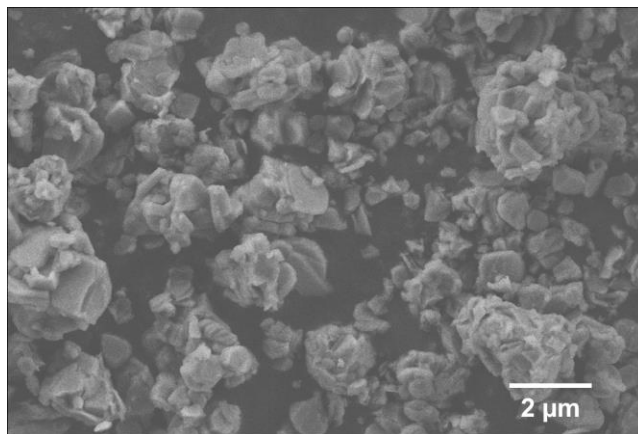


Figure S1. SEM image of P3-K_{0.5}MnO₂.

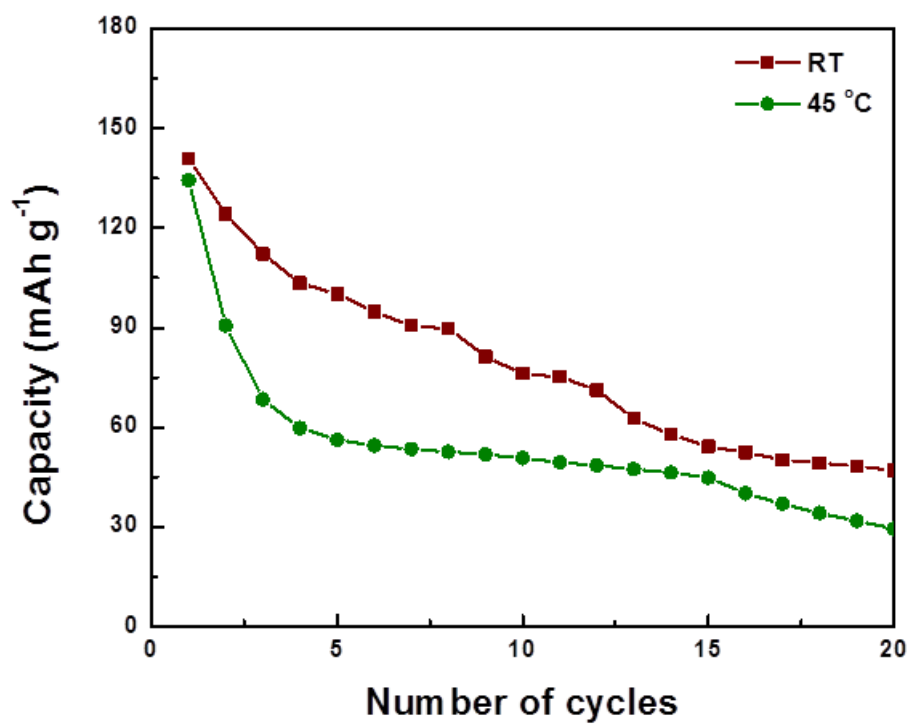


Figure S2. Discharge capacities of P3-type $\text{K}_{0.5}\text{MnO}_2$ over 20 cycles operated at RT and 40 °C at a current rate of 5 mA g^{-1} .

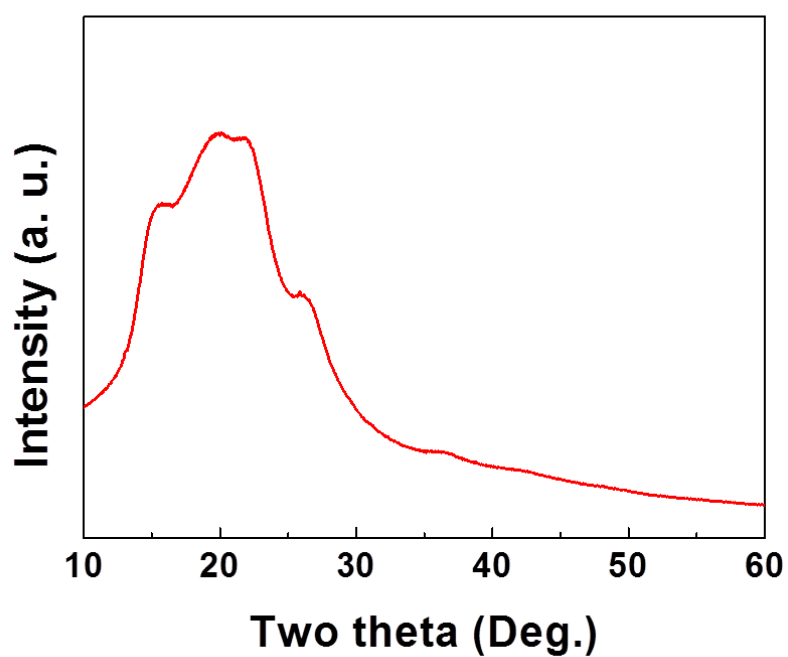


Figure S3. *Ex-situ* XRD of $K_{0.5}MnO_2$ after high voltage cycling. Note that the large background between 12° to 30° originates from the Kapton film used to seal the sample.

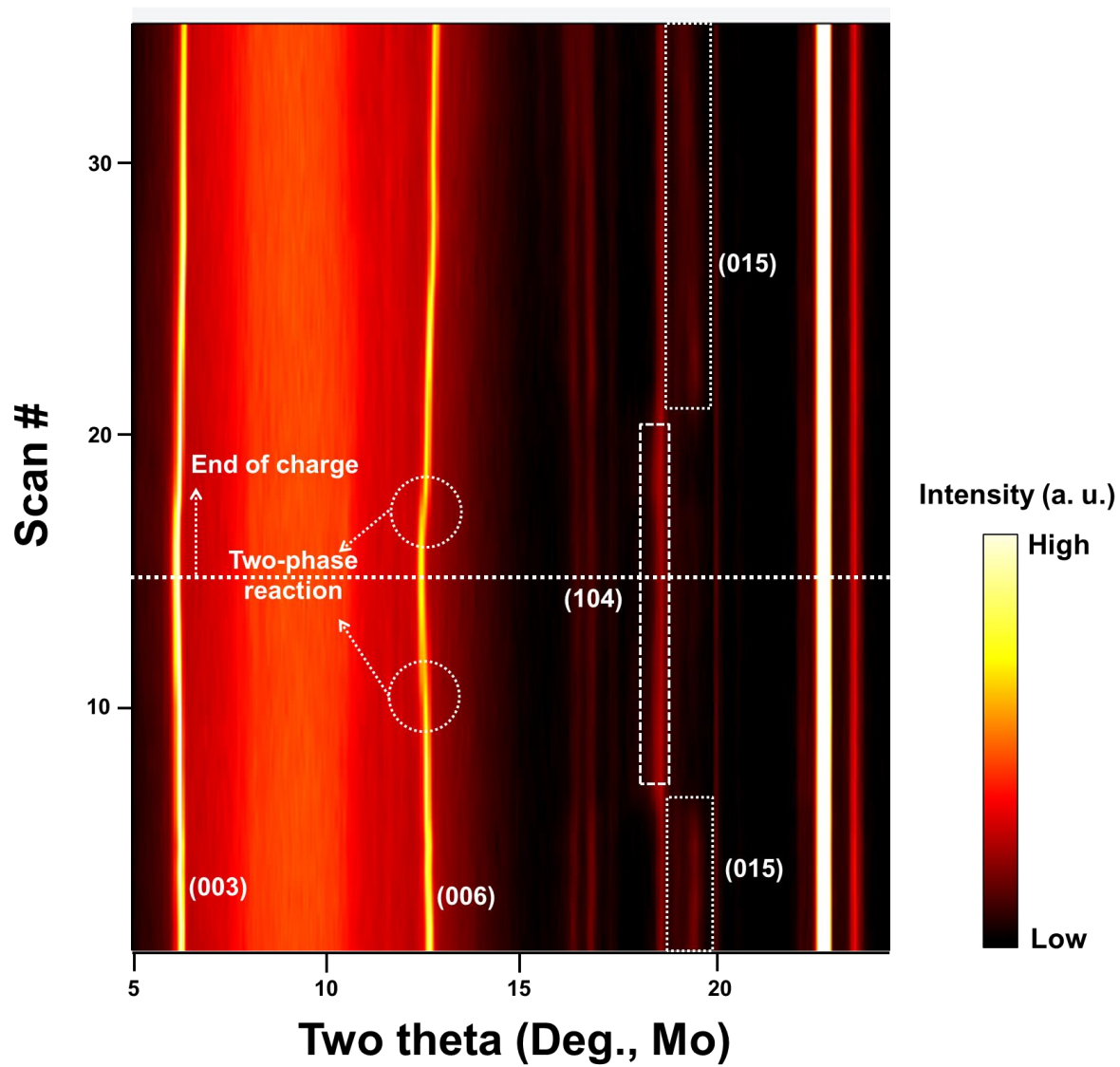


Figure S4. 2D plot of *in situ* XRD characterization.

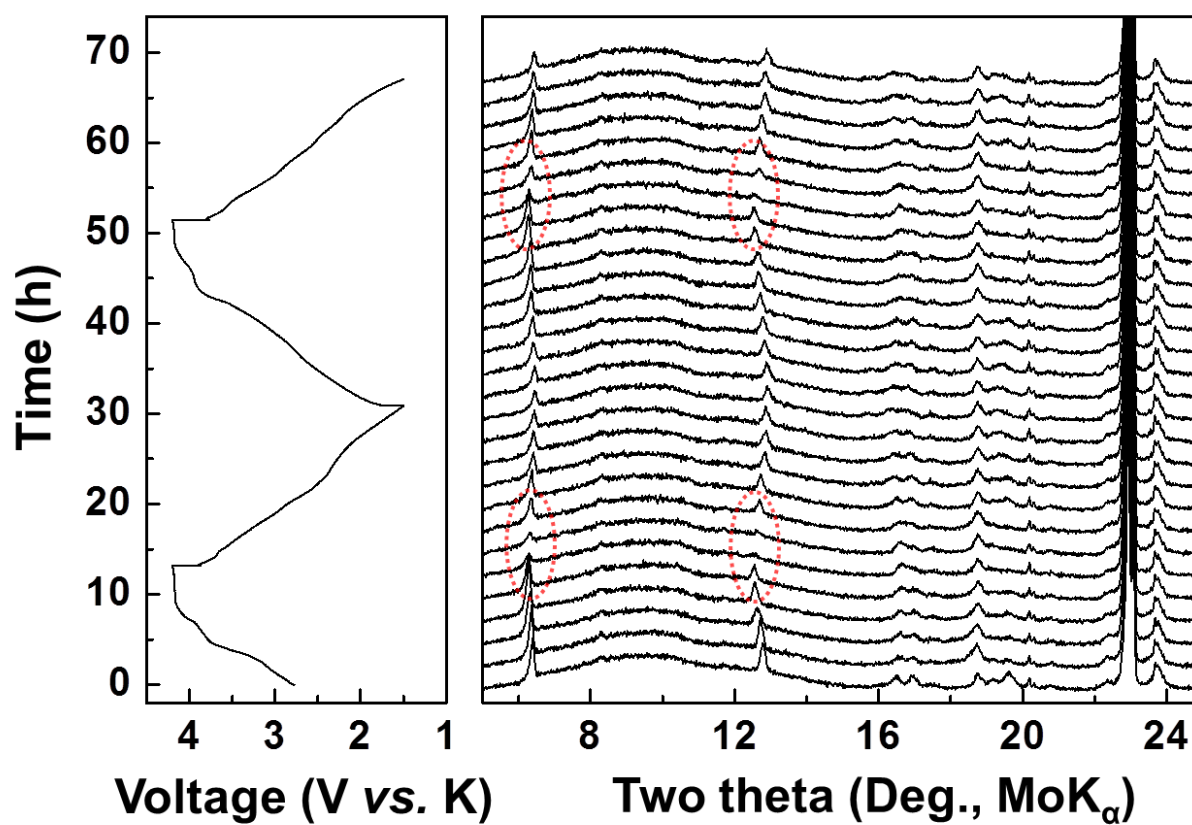


Figure S5. Typical charge/discharge profiles of P3-type $\text{K}_{0.5}\text{MnO}_2$ at a current rate of 7 mA g^{-1} between 1.5–4.2 V and corresponding *in situ* XRD patterns.

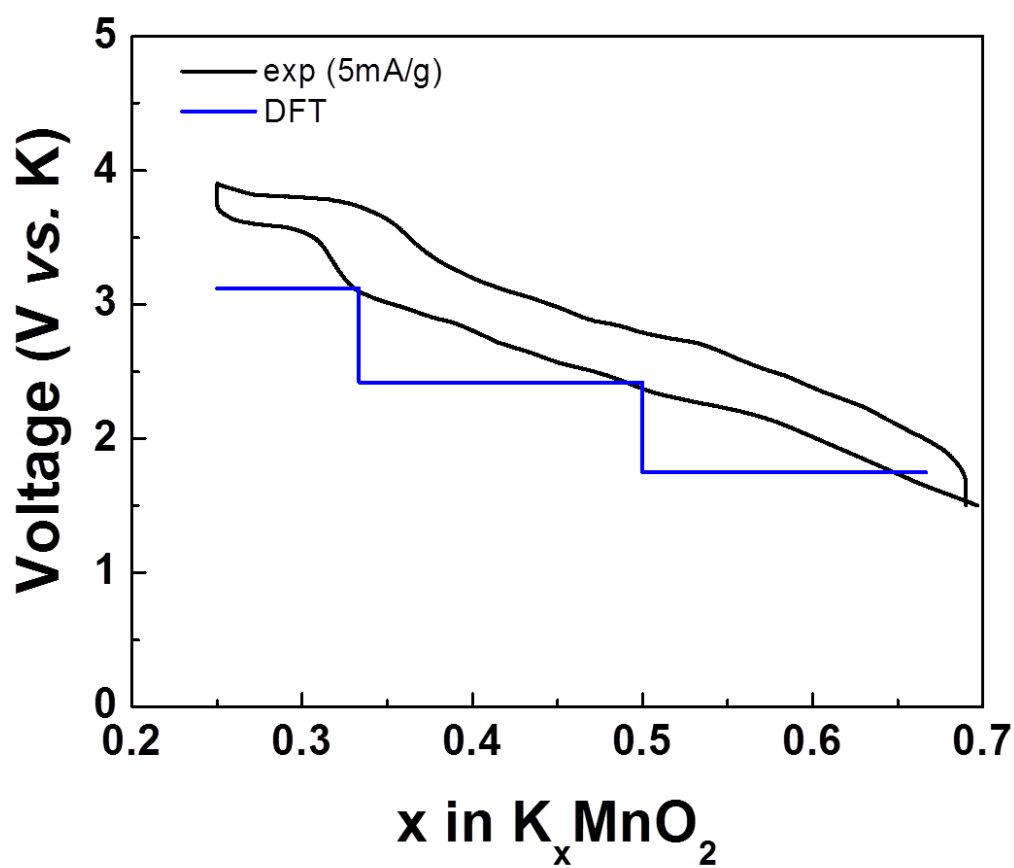


Figure S6. Calculated voltage plot (DFT) compared with experimentally obtained charge/discharge profiles.